Accurate and Fast Analysis of Reflective Surfaces and Metasurface Antennas With Sheet Impedance Boundary Conditions

Jean Cavillot, *Member, IEEE*, Modeste Bodehou, *Member, IEEE*, Adam Abazi, *Graduate Student Member, IEEE*, and Christophe Craeye, *Senior Member, IEEE*

***Abstract*—Simulating the fine geometry of metasurface (MTS) structures in a conventional way is a difficult task requiring huge computational resources. On the other hand, the metallization can usually be modeled as an impedance sheet with a modulation scale of the order of the operating wavelength. Even then, direct solution of the system of equations is usually not possible due to memory saturation. As a consequence, one has to resort to iterative methods. However, the analysis of an impedance sheet lying on a grounded slab based on an iterative solution of the method of moments (MoM) may lead to ill-conditioning and a large number of iterations. This is certainly the case when the range of impedance spans both the capacitive and inductive domains. Such an impedance range is, in practice, required for reflective intelligent surfaces (RISs) and for some MTS antennas. This article proposes a preconditioner aiming to solve bad convergence issues caused by the wide range of the surface impedance. The preconditioner involves a multiplication by the conjugate of the MoM matrix, followed by a block diagonal preconditioner. The block diagonal preconditioner has memory and multiplication complexity $N^{3/2}$. It is precalculated in an accelerated scheme relying on FFTs. Besides, multiplication with the MoM matrix is carried out with complexity $N\log(N)$, thanks to the use of FFTs.**

***Index Terms*—Fast Fourier transform (FFT), impedance boundary condition (IBC), metasurface antennas, method of moments (MoM), reflective intelligent surfaces (RISs), Toeplitz matrices.**

I. Introduction

REFLECTIVE intelligent surfaces (RISs) [1] and metasurface (MTS) antennas [2] are currently at the center of attention of the antenna and propagation community. RISs are often described as a key factor for the success of the sixth-generation wireless communications due to their ability to engineer the propagation channel through manipulation of reflected fields [3]. Low-profile MTS antennas, on the other hand, are designed to generate radiating fields leaking from a surface wave (SW) [2], [4]. The feeder being incorporated in the metasurfaces (MTS) substrate, MTS antennas are particularly suited for applications requiring high gain with low-profile and low-cost platforms. Both technologies have recently experienced rapid development. For example, anomalous reflection has been demonstrated in [5], and multibeam reflection has been shown in [6] and [7] using RISs. MTS antennas designed for pencil beam [8], multibeaming [9], [10], and shaped beams [4] have also been reported in the literature. All these meta-structures share a feature: the MTS and the RIS are usually realized with a dense texture of subwavelength metallization printed on a grounded slab. The metallization layer implements a smooth impedance sheet distribution over the surface. While being numerically easier to analyze when compared to the simulation of the physical structure of the MTS, several articles have shown that the sheet impedance model of the printed metallization provides an accurate prediction of the fields because it properly accounts for the spatial dispersion of the grounded slab [11], [12]. Despite the drastic reduction in the number of unknowns in the sheet impedance formulation, direct solving by Gaussian elimination becomes rapidly impractical due to memory saturation when the size of the MTS exceeds a few wavelengths. Therefore, fast and memory-efficient simulation methods have been developed using the sheet impedance model in an electric field integral equation (EFIE) formalism [13], [14], [15], [16] based on the method of moments (MoM) [17]. Although the resulting system of equations matrix is particularly well-conditioned for strongly capacitive sheet impedances (as is usually the case for large-aperture MTS antennas), conditioning issues rapidly appear when dealing with an impedance distribution spanning from capacitive to inductive (or even low reactance capacitive) [12], [16]. Such impedance ranges are, in practice, useful for RISs [11], [18]. Low reactance capacitive impedances can be adopted for improving the feeder efficiency of MTS antennas [19]. In this article, we designate by "low reactance capacitive impedance," a reactive impedance with a negative imaginary part which does not exceed a few hundred ohms. The conditioning problems associated with such impedances prevent the use of iterative solvers because the convergence becomes very slow.

It is well known that the conditioning of the EFIE MoM system of equations matrix deteriorates when approaching low frequency or with growing discretization density [20].

Received 28 June 2024; revised 25 August 2025; accepted 21 September 2025. Date of publication 8 October 2025; date of current version 18 December 2025. This work was supported in part by Belgium Fonds National de la Recherche Scientifique (F.R.S.-FNRS) and in part by the HORIZON EUROPE European Innovation Council (EIC) Pathfinder Open Program "Flexible Intelligent Near-Field Sensing Skins (FITNESS)" funded by the European Union under Grant 101098996. *(Corresponding author: Jean Cavillot.)*

Jean Cavillot, Adam Abazi, and Christophe Craeye are with the University of UCLouvain, 1348 Louvain-la-Neuve, Belgium (e-mail: jean.cavillot@uclouvain.be).

Modeste Bodehou is with the Research Unit in Photonics and Wireless Communications, LETIA/EPAC, Université d'Abomey-Calavi, Abomey-Calavi, Benin.

Digital Object Identifier 10.1109/TAP.2025.3617109

Over the past few decades, several approaches have been developed to solve this issue. Considering antenna arrays of identical elements, enhanced versions of the block diagonal preconditioner can be used to improve the condition number of the MoM matrix [21], [22]. Conditioning can also be improved using the generalized shielded block preconditioner, by dividing the whole structure into overlapping subdomains [23], [24]. These preconditioners are, however, very demanding in terms of memory allocation and are not fit for dense and connected structures in layered media [25]. Another class of preconditioners has been developed using the Calderon identities [26], [27]. Calderon preconditioners exploit the self-regularizing properties of the EFIE by invoking the square of the EFIE operator. An extension of the Calderon preconditioner including uniform surface impedance is provided in [28]. However, to the best of the authors' knowledge, this method has not been extended to MTS antennas and RIS modeled as tensor sheet impedances. An article proposing a different approach has been recently published in [29]. In the latter, the authors tackle the ill-conditioning for the specific case of scalar and spatially constant sheet impedance by using a regularization scheme based on entire-domain basis functions.

The present article proposes a preconditioner adapted to the analysis of a wide range of modulated sheet impedance lying on a grounded slab, as required for RIS and MTS antennas. Slow convergence has been observed in the past when the impedance range approaches the inductive domain. This includes large perfect electrical conductors (PECs) printed on a grounded substrate, which corresponds to the case where the sheet impedance is zero. As explained in [30], the convergence of an iterative solver such as the generalized minimal RESidual (GMRES) solver can be dramatically impacted by the clustering of the eigenvalues. For example, faster convergence is usually observed when the eigenvalues are located on the positive real axis. Accordingly, the proposed preconditioner significantly improves the convergence of the iterative solver by first redistributing the eigenvalues on the positive real axis after left-multiplying with the conjugate of the original matrix using fast Fourier transforms (FFTs), hence with an $O(N \log N)$ complexity. In a second step, a block diagonal preconditioner, which keeps the eigenvalues on the positive real axis, is applied. Besides, FFTs are also used to precalculate the block diagonal preconditioner. Considering a square-shaped domain, this matrix has memory and matrix–vector multiplication complexities of $O(N^{3/2})$. The fast convergence, along with the fast matrix–vector multiplications, enables the analysis of finite MTSs. Consequently, an MTS of size larger than ten wavelengths, described with hundreds of thousands of basis functions, can be analyzed in less than one hour. Besides, accurate results are obtained with respect to the ones obtained by direct inversion of the initial system of equations. The presented method can also be easily extended to MTSs with arbitrary shapes, as shown in [31]. The article is structured as follows. Section II briefly recalls a fast MoM formulation adapted to high reactance capacitive IBCs. Section III presents the proposed preconditioner, and Section V provides numerical results.

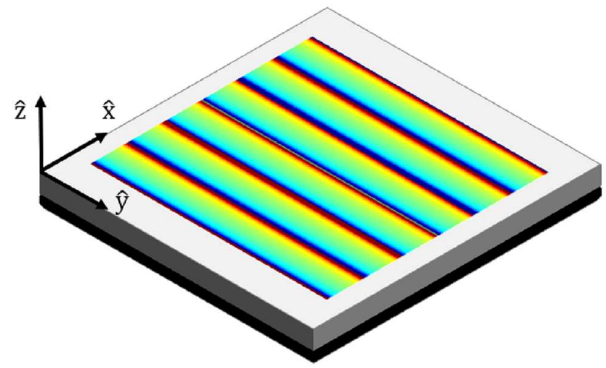

Fig. 1. Schematic illustration of an MTS modeled as a sheet IBC lying on a grounded slab.

II. Method of Moments Formulation

Let us consider an RIS or an MTS modeled as a sheet impedance boundary condition (IBC) lying on a grounded substrate, as depicted in Fig. 1. A Cartesian system of coordinates is adopted with unit vectors $\hat{\boldsymbol{x}}$ and $\hat{\boldsymbol{y}}$ on the surface. Using the surface equivalence theorem, the sheet IBC can be replaced by an equivalent surface current distribution expanded into a set of basis functions as

$$\mathbf{J}\left(\boldsymbol{r}'\right) = \sum_{n=1}^{N} i_n \, \mathbf{j}_n\left(\boldsymbol{r}'\right) \tag{1}$$

where $\mathbf{j}_n(\boldsymbol{r}')$ corresponds to the n^{th} basis function, $\boldsymbol{r}' = (x', y')$ is a vector providing the local coordinates on the surface, and i_n is the unknown weight associated with the n^{th} basis function. The sheet IBC $\underline{\underline{\mathbf{Z_s}}}$ imposes a direct relation between the average electric field $\overline{\mathbf{E}}_{\mathbf{av}}$ on the surface and the equivalent surface current

$$\hat{\mathbf{n}} \times \mathbf{E_{av}} = \hat{\mathbf{n}} \times \left(\underline{\underline{\mathbf{Z_s}}} \cdot \mathbf{J}\right) \tag{2}$$

where $\hat{\mathbf{n}}$ is the normal to the surface. The electric field to be averaged corresponds to the sum of the incident field $\mathbf{E}^{\text{inc}}$, which depends on the excitation, and the fields scattered by the MTS, $\mathbf{E}^{\text{scat}}$. The latter can be obtained from the convolution between the equivalent surface current and the medium Green's function $\underline{\underline{\mathbf{G}}}^{EJ}(\boldsymbol{r}, \boldsymbol{r}')$

$$\hat{\mathbf{n}} \times \mathbf{E_{av}} = \hat{\mathbf{n}} \times \left(\mathbf{E}^{\text{inc}} + \mathbf{E}^{\text{scat}}\right) \tag{3}$$

$$= \hat{\mathbf{n}} \times \mathbf{E}^{\text{inc}} + \hat{\mathbf{n}} \times \iint_{S'} \underline{\underline{\mathbf{G}}}^{EJ}\left(\boldsymbol{r}, \boldsymbol{r}'\right) \; \mathbf{J}\left(\boldsymbol{r}'\right) \; \mathrm{d}S' \tag{4}$$

where it has been assumed that the MTS sheet is thin enough for the electric field to be considered continuous across the sheet [12]. The electric field is tested with a set of testing functions corresponding to the chosen set of basis functions (Galerkin testing). From there, the following equations are obtained:

$$\begin{aligned}&\iint_{S} \mathbf{j}_m\left(\boldsymbol{r}\right) \cdot \mathbf{E}^{\text{inc}} \; \mathrm{d}S \\ &\quad + \sum_{n=1}^{N} i_n \iint_{S} \mathbf{j}_m\left(\boldsymbol{r}\right) \iint_{S'} \underline{\underline{\mathbf{G}}}^{EJ}\left(\boldsymbol{r}, \boldsymbol{r}'\right) \;\; \mathbf{j}_n\left(\boldsymbol{r}'\right) \; \mathrm{d}S' \; \mathrm{d}S \\ &= \sum_{n=1}^{N} i_n \iint_{S} \mathbf{j}_m\left(\boldsymbol{r}\right) \; \underline{\underline{\mathbf{Z_s}}}\left(\boldsymbol{r}\right) \; \mathbf{j}_n\left(\boldsymbol{r}'\right) \; \mathrm{d}S \quad m = 1, 2, \ldots, N\end{aligned} \tag{5}$$

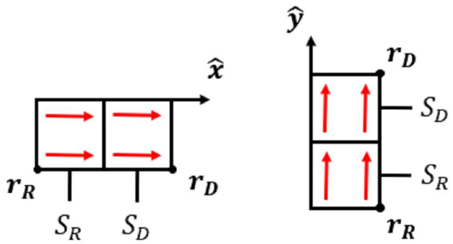

Fig. 2. x-oriented and y-oriented rooftop basis functions.

which can be written in the following matrix form:

$$(\mathbf{Z_G} - \mathbf{Z_{IBC}})\ \mathbf{I} = \mathbf{V} \tag{6}$$

where $\mathbf{Z}_G$ is the substrate matrix whose entries are given by

$$Z_G(n,m) = \iint \boldsymbol{j}_n(\boldsymbol{r}') \iint \underline{\underline{\mathbf{G}}}^{EJ}(|\boldsymbol{r}-\boldsymbol{r}'|)\ \boldsymbol{j}_m(\boldsymbol{r})\ dS'dS \tag{7}$$

and where the entries of the IBC matrix $\mathbf{Z}_{IBC}$ are given by

$$Z_{IBC}(n,m) = \iint \boldsymbol{j}_n(\boldsymbol{r})\ \underline{\underline{\mathbf{Z}}}_S(\boldsymbol{r})\ \boldsymbol{j}_m(\boldsymbol{r})\ dS. \tag{8}$$

Finally, the entries of the excitation vector $\mathbf{V}$ are obtained after testing the excitation field

$$V(m) = -\iint \mathbf{E}^{\text{inc}} \cdot\ \boldsymbol{j}_m(\boldsymbol{r})\ dS. \tag{9}$$

In this article, x-oriented and y-oriented rooftop basis functions [32] are used

$$\boldsymbol{j}_n(\boldsymbol{r}') = \begin{cases} \dfrac{(\boldsymbol{r}'-\boldsymbol{r}_p)\cdot\hat{\boldsymbol{n}}_j}{h_p}\hat{\boldsymbol{n}}_j\cdot & \text{if } x \in S_p \\ 0, & \text{otherwise} \end{cases} \tag{10}$$

where the subscript p denotes the rising (R) or the decaying (D) part of the basis function, as shown in Fig. 2; h_p is the height of the half basis function. Bold fonts are used to denote vectors. The outer normal to the surface $\hat{\boldsymbol{n}}_j$ corresponds to $\hat{\boldsymbol{x}}$ for x-oriented basis functions and to $\hat{\boldsymbol{y}}$ for y-oriented basis functions. S_j is the surface of the half basis function. The length of the basis function is set to $\lambda_0/10$, where λ_0 is the free-space wavelength. A regular grid of x-oriented and y-oriented basis functions is used as in [16]. A schematic representation of the mesh is given in Fig. 3, where the relative size of the rooftop basis functions is exaggerated for clarity. The regularity of the mesh allows one to exploit the structure of the substrate matrix $\mathbf{Z}_G$ for faster solution. Let us consider the mesh as N_x shifted rows of n_x x-oriented basis functions and N_y shifted rows of n_y y-oriented basis functions; hence, a total of $N_x \times n_x$ x-oriented basis functions and $N_y \times n_y$ y-oriented basis functions. In this case, the substrate matrix can be divided into four Toeplitz–Block Block–Toeplitz (TBBT) submatrices [16]

$$\mathbf{Z}_G = \left[\begin{array}{c|c} \mathbf{T}^{xx} & \mathbf{T}^{xy} \\ \hline \mathbf{T}^{yx} & \mathbf{T}^{yy} \end{array}\right] \tag{11}$$

where $\mathbf{T}^{xx}$ and $\mathbf{T}^{yy}$ are the matrices of self-interaction of x-oriented and y-oriented basis functions, respectively. The off-diagonal matrices account for the coupling between x-oriented and y-oriented basis functions. Each of these submatrices has a TBBT structure

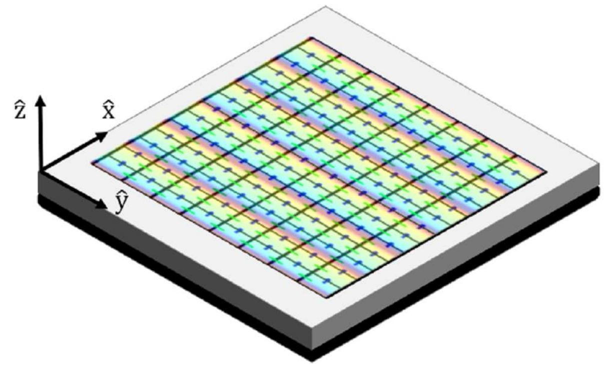

Fig. 3. Illustration of a sheet IBC meshed with rooftop basis functions.

$$\mathbf{T}^{ij} = \begin{bmatrix} \mathbf{T}_{11}^{ij} & \mathbf{T}_{12}^{ij} & \cdots & \cdots & \mathbf{T}_{1N_j}^{ij} \\ \mathbf{T}_{21}^{ij} & \mathbf{T}_{11}^{ij} & \mathbf{T}_{12}^{ij} & \cdots & \mathbf{T}_{2N_j}^{ij} \\ \vdots & \mathbf{T}_{21}^{ij} & \mathbf{T}_{11}^{ij} & \ddots & \vdots \\ \vdots & \ddots & \ddots & \ddots & \mathbf{T}_{12}^{ij} \\ \mathbf{T}_{N_i1}^{ij} & \mathbf{T}_{N_i2}^{ij} & \cdots & \mathbf{T}_{21}^{ij} & \mathbf{T}_{11}^{ij} \end{bmatrix} \tag{12}$$

where i and j are either x or y. All the submatrices $\mathbf{T}^{ij}$ are Toeplitz. Thanks to the structural properties of matrix $\mathbf{Z}_G$, the filling of this matrix is fast and grows with linear complexity with respect to the number of unknowns [16]. Indeed, knowing the first column (or row) of each of the four submatrices of $\mathbf{Z}_G$ is sufficient to know the entire matrix. Regarding the IBC matrix, nonzero entries only concern overlapping basis functions. Hence, the matrix $\mathbf{Z}_{IBC}$ is highly sparse. As explained in [16], the structure of the matrices can be exploited to perform fast matrix–vector multiplications in an iterative search for the solution. Multiplying by a TBBT matrix can be seen as a 2-D convolution [33] and hence can be performed with 2-D FFTs. Besides, multiplying by the IBC matrix is fast, given its sparse structure, and can be achieved with linear complexity. Overall, a matrix–vector multiplication with the system matrix given in (6) can be achieved with N logN complexity. Provided that the system of equations is well-conditioned, this feature can be exploited in iterative solvers such as GMRES [34], as done in [16].

III. Preconditioning and Solution

The linear system of equations (6) is well conditioned when considering MTSs with highly capacitive sheet IBCs [12]. However, the system becomes ill-posed when the sheet impedance gets closer or enters the inductive range [12], [16], [35]. In this article, we propose the usage of a preconditioner $\mathbf{P}$ defined as

$$\mathbf{P} = \mathbf{iD}\ (\mathbf{Z_G} - \mathbf{Z_{IBC}})^H \tag{13}$$

where H denotes the conjugate transpose operator, and $\mathbf{iD}$ is a block diagonal preconditioner defined as

$$\mathbf{iD} = \left[\begin{array}{c|c} \mathbf{iD}^{xx} & \mathbf{0} \\ \hline \mathbf{0} & \mathbf{iD}^{yy} \end{array}\right]. \tag{14}$$

The matrix $\mathbf{iD}^{xx}$ is composed of N_x submatrices of size $n_x \times n_x$ and the matrix $\mathbf{iD}^{yy}$ is composed of N_y submatrices of size $n_y \times n_y$

$$\mathbf{iD}^{ii} = \begin{bmatrix} \mathbf{iD}_1^{ii} & \mathbf{0} & \cdots & \cdots & \mathbf{0} \\ \mathbf{0} & \mathbf{iD}_2^{ii} & \mathbf{0} & \cdots & \mathbf{0} \\ \vdots & \mathbf{0} & \ddots & \ddots & \vdots \\ \vdots & \vdots & \ddots & \ddots & \vdots \\ \mathbf{0} & \mathbf{0} & \cdots & \mathbf{0} & \mathbf{iD}_{N_i}^{ii} \end{bmatrix} \quad (15)$$

where i is either x or y. Considering a square domain, this matrix has memory complexity $O(N^{3/2})$, with N being the total number of basis functions. Each block diagonal submatrix in $\mathbf{iD}^{ii}$ is obtained after inverting the corresponding block diagonal of the matrix $\mathbf{Z} = (\mathbf{Z}_G - \mathbf{Z}_{IBC})^H(\mathbf{Z}_G - \mathbf{Z}_{IBC})$. In other words, if we define the operator $\mathcal{D}\{\cdot\}$ which selects the first N_x block diagonals of size $n_x \times n_x$ and the following N_y block diagonals of size $n_y \times n_y$ of a given matrix, $\mathbf{iD}$ is given by

$$\mathbf{iD} = \mathcal{D}\{\mathbf{Z}\}^{-1} \quad (16)$$

where the superscript -1 denotes the matrix inverse. That means, rather than solving (6), we are actually solving

$$\mathbf{iD}\,(\mathbf{Z_G} - \mathbf{Z_{IBC}})^{\mathbf{H}}\,(\mathbf{Z_G} - \mathbf{Z_{IBC}})\,\mathbf{I} = \mathbf{iD}\,(\mathbf{Z_G} - \mathbf{Z_{IBC}})^{\mathbf{H}}\,\mathbf{V}. \quad (17)$$

In an iterative solving of (17), one needs to compute at each iteration a product between the matrix $\mathbf{iD} \times (\mathbf{Z}_G - \mathbf{Z}_{IBC})^H(\mathbf{Z}_G - \mathbf{Z}_{IBC}) = \mathbf{iD} \times \mathbf{Z}$ and a given vector $\mathbf{U}$. This product can be computed extremely fast without explicitly computing $\mathbf{Z}$. Indeed, first, the product $\mathbf{ZU}$ is computed after expanding $\mathbf{Z}$ as

$$\mathbf{Z} = \mathbf{Z}_G^H\mathbf{Z}_G - \mathbf{Z}_G^H\mathbf{Z}_{IBC} - \mathbf{Z}_{IBC}^H\mathbf{Z}_G + \mathbf{Z}_{IBC}^H\mathbf{Z}_{IBC} \quad (18)$$

while noting that multiplying by $\mathbf{Z_G}^H$ can also be carried out using 2-D FFTs, and multiplication with $\mathbf{Z}_{IBC}^H$ is extremely fast given its sparsity.

The block diagonal preconditioner $\mathbf{iD}$ can be obtained by selecting, summing, and then inverting the block diagonals of the four terms in (18)

$$\mathbf{iD} = \Big(\mathcal{D}\left\{\mathbf{Z}_G^H\mathbf{Z}_G\right\} - \mathcal{D}\left\{\mathbf{Z}_G^H\mathbf{Z}_{IBC}\right\} \quad (19)$$

$$-\mathcal{D}\left\{\mathbf{Z}_{IBC}^H\mathbf{Z}_G\right\} + \mathcal{D}\left\{\mathbf{Z}_{IBC}^H\mathbf{Z}_{IBC}\right\}\Big)^{-1} \quad (20)$$

$$= \left(\mathbf{D}^{GG} - \mathbf{D}^{GI} - \mathbf{D}^{GI,H} + \mathbf{D}^{II}\right)^{-1} \quad (21)$$

$$= \left(\mathbf{D}^{GG} + \mathbf{D}^{IBC}\right)^{-1} \quad (22)$$

where all the IBC-dependent matrices have been grouped in $\mathbf{D}^{IBC}$. The first block diagonal of size $n_x \times n_x$ is obtained by inverting the sum of four block diagonals, each of size $n_x \times n_x$ corresponding to the first block diagonal of the four matrices in (18)

$$\mathbf{iD}_1^{xx} = \left(\mathbf{D}_1^{GG,xx} - \mathbf{D}_1^{GI,xx} - \mathbf{D}_1^{GI,xx,H} + \mathbf{D}_1^{II,xx}\right)^{-1} \quad (23)$$

where the third term is the conjugate transpose of the second one. Let us focus on the first term, which does not depend on the sheet impedance. This term can be obtained by performing a block-by-block multiplication of matrices $\mathbf{Z_G}$ and $\mathbf{Z_G}^H$. Thus, the first block diagonal of $\mathbf{D}^{GG}$ can be obtained as follows:

$$\mathbf{D}_1^{GG,xx} = \sum_{i=1}^{N_x}\mathbf{T}_{1i}^{xx,H}\mathbf{T}_{i1}^{xx} + \sum_{i=1}^{N_y}\mathbf{T}_{1i}^{xy,H}\mathbf{T}_{i1}^{yx} \quad (24)$$

where each matrix–matrix multiplication can be accelerated with the FFT. It is important to note that, thanks to the block Toeplitz matrix properties, the jth block $\mathbf{D}_j^{GG,xx}$ can be obtained from minor additional operations on the previous block $\mathbf{D}_{j-1}^{GG,xx}$, for example,

$$\mathbf{D}_2^{GG,xx} = \sum_{i=1}^{N_x}\mathbf{T}_{2i}^{xx,H}\mathbf{T}_{i2}^{xx} + \sum_{i=1}^{N_y}\mathbf{T}_{2i}^{xy,H}\mathbf{T}_{i2}^{yx} \quad (25)$$

$$= \mathbf{D}_1^{GG,xx} - \mathbf{T}_{1N_x}^{xx,H}\mathbf{T}_{N_x1}^{xx} + \mathbf{T}_{12}^{xx,H}\mathbf{T}_{21}^{xx} \quad (26)$$

$$- \mathbf{T}_{1N_x}^{xy,H}\mathbf{T}_{N_x1}^{yx} + \mathbf{T}_{12}^{xy,H}\mathbf{T}_{21}^{yx}. \quad (27)$$

The terms related to the IBC matrix can also be obtained using FFTs and exploiting the sparse structure of $\mathbf{Z}_{IBC}$. Let us consider an anisotropic sheet impedance, in this case $\mathbf{D}_{11}^{GI,xx}$ can be obtained as

$$\mathbf{D}_{11}^{GI,xx} = \mathbf{T}_{11}^{xx,H}\mathbf{Z}_{IBC,11}^{xx} + \mathbf{T}_{11}^{xy,H}\mathbf{Z}_{IBC,11}^{xy} \quad (28)$$

where we used the same block designation as in (11) for the $\mathbf{Z}_{IBC}$ matrix and FFTs can be used to compute the matrix–matrix multiplication. Finally, the block diagonal $\mathbf{D}_{11}^{II,xx}$ can be obtained by multiplying sparse blocks of the IBC matrix and of its conjugate

$$\mathbf{D}_{11}^{II,xx} = \mathbf{Z}_{IBC,11}^{xx,H}\mathbf{Z}_{IBC,11}^{xx} + \mathbf{Z}_{IBC,11}^{xy,H}\mathbf{Z}_{IBC,11}^{xy}. \quad (29)$$

The same strategy can be applied to rapidly obtain all the remaining diagonal blocks of the preconditioner.

Once the preconditioner has been calculated, the following new system of equations can be solved using GMRES

$$\mathbf{iD}\ \mathbf{Z}\ \mathbf{I} = \mathbf{iD}\ (\mathbf{Z_G} - \mathbf{Z_{IBC}})^H\mathbf{V} \quad (30)$$

where $\mathbf{Z}$ and $\mathbf{Z}_G$ are never explicitly calculated.

IV. Eigenvalues, Preconditioner Block Size, and Discretization

The proposed preconditioner significantly accelerates the convergence of the iterative solver. One of the reasons is that the eigenvalues of $\mathbf{iD}\ \mathbf{Z}$ are clustered on the positive real axis. In this section, we consider three isotropic homogeneous sheets of impedance: 1) highly capacitive (-500j Ω)): 2) zero-impedance [perfect electric conductor (PEC)]; and 3) highly inductive [500j Ω)]. We show the distribution of the eigenvalues of both the initial and the proposed system of equations in Fig. 4. The three sheets of impedance lie on a grounded substrate of relative permittivity $\epsilon_r = 3.66$ and thickness $d = 1.524$ mm. The sheet impedance is imposed on a $3.2\lambda_0 \times 3.2\lambda_0$ domain and a frequency of 24 GHz is considered. Considering first the capacitive case, the eigenvalues cluster away from zero, and the initial system of equations is usually well-conditioned. In the PEC and the inductive cases, the eigenvalues of the MoM system span both the positive and negative parts of the imaginary plane and approach zero, thus

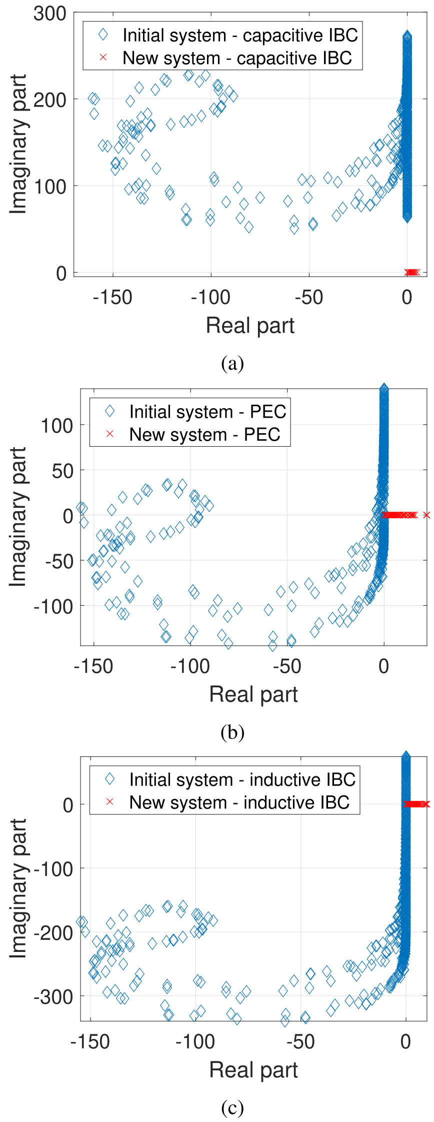

Fig. 4. Distribution of the eigenvalues for the initial EFIE-IBC system of equations (blue) and for the preconditioned system (red) considering (a) capacitive IBC, (b) zero IBC (PEC), and (c) inductive IBC.

TABLE I

REQUIRED NUMBER OF ITERATIONS TO REACH A RESIDUAL NORM OF 1E-6

Discretization	$\lambda_0/10$			$\lambda_0/5$		
Preconditioner	None	$\mathbf{P}$	$\mathbf{P_2}$	None	$\mathbf{P}$	$\mathbf{P_2}$
Capacitive	31	29	29	27	28	27
Metal	526	219	197	404	179	194
Inductive	1001	457	333	73	65	72

leading to ill-conditioning. However, the eigenvalues always cluster on the positive real axis when using the proposed preconditioner. The impact of finer discretization and of the block diagonal preconditioner size on the convergence is shown in Table I. The number of iterations required for GMRES to reach a residual norm of 1e-6 for the three aforementioned sheet impedances. Two discretization densities are considered: $\lambda_0/10$ and $\lambda_0/5$. The required number of iterations is also given when the block size of the block diagonal matrix $\mathbf{iD}$ is doubled in (15). In this case, the preconditioner is noted $\mathbf{P_2}$. In the capacitive case, finer discretization does not seem to impact the convergence, while it clearly does for the PEC and inductive cases. Finally, it can be observed that using a preconditioner with a larger block size than the one given in (15) does not necessarily reduce the required number of iterations (while it does increase the required memory storage). For the rest of the article, the discretization is set to $\lambda_0/10$ and the block size of (15) indicated in Section III is used.

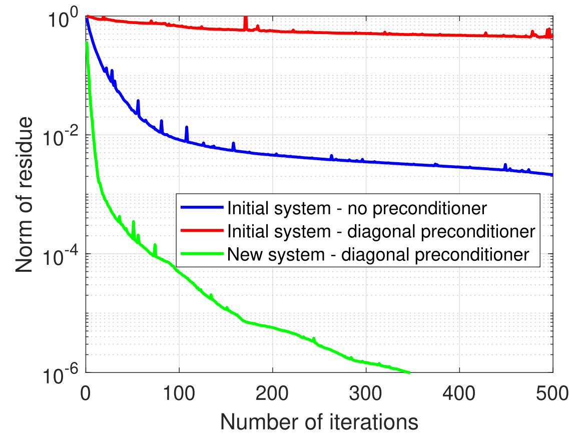

Fig. 5. GMRES convergence: the proposed preconditioned system of equations (29) is compared with the initial system (6) with and without the diagonal preconditioner.

V. Numerical Examples

This section provides analysis results of RIS and MTS antennas with the proposed preconditioner.

A. RIS Analysis

Let us consider an RIS operating at 24 GHz. The RIS lies on a grounded slab with relative permittivity $\epsilon_r = 3.5$ and thickness $d = 1.524$ mm. The dimensions of the MTS are fixed to $7\lambda_0$ in the x-direction and $4\lambda_0$ in the y-direction. The isotropic sheet impedance distribution derived from the desired local reflection coefficient is given by

$$Z_s(x) = -j\frac{Z_0}{\tan\left(\frac{kx\sin\theta_r}{2}\right) + \sqrt{\epsilon_r}\cot\left(k\sqrt{\epsilon_r}d\right)} \tag{31}$$

with $Z_0 = 376.73\ \Omega$ being the free-space impedance and k is the free-space wavenumber at the operating frequency. This sheet impedance distribution provides the linear phase evolution $(\exp(-jkx\sin\theta_r)$ [36]) required to transform an incident TM-polarized beam from broadside to a reflected TM-polarized beam in a direction θ_r, in the plane $y = 0$. A Gaussian incident field $\mathbf{E}_i$ from broadside is considered, with expression at the MTS level given by

$$\mathbf{E}_i(x, y) = \mathrm{e}^{-(x^2/(2s_x^2)+y^2/(2s_y^2))}\hat{\mathbf{x}} \tag{32}$$

with $s_x = 1.4\lambda_0$ and $s_y = 0.8\lambda_0$. A reflection angle $\theta_r = 20°$ is targeted. The convergence of the initial system of equations (6) with and without diagonal preconditioner is compared to the convergence of the new system of equations (30) in Fig. 5. As observed, the proposed preconditioner significantly improves the convergence while a conventional diagonal preconditioner,

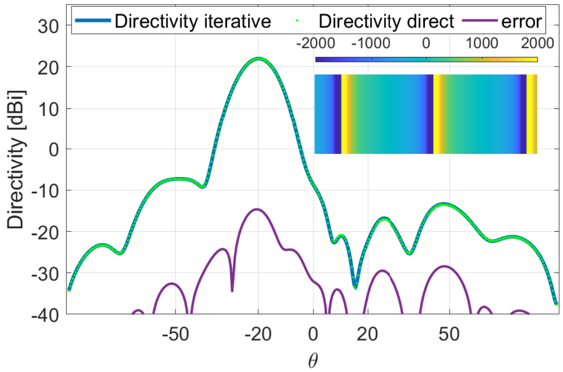

Fig. 6. Radiation pattern of the $7\lambda_0 \times 4\lambda_0$ RIS generating anomalous reflection at 20°. The result of the presented iterative method is compared to direct solving. The error in dB between the results is provided. The inset provides the imaginary part of the sheet impedance.

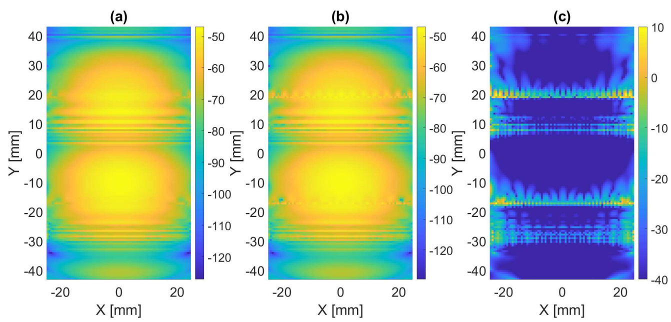

Fig. 7. Equivalent currents obtained on the RIS surface using (a) iterative method and (b) direct solving. (c) Relative error between both currents in dB.

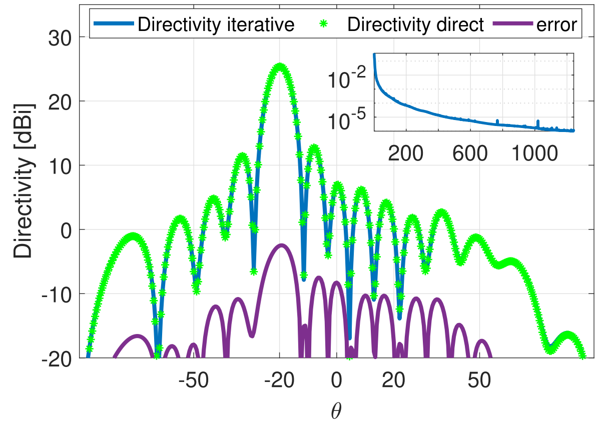

Fig. 8. Radiation pattern of the $7\lambda_0 \times 4\lambda_0$ RIS generating anomalous reflection at 20° when excited by a broadside impinging plane wave. The inset shows the convergence of GMRES with the proposed system of equations.

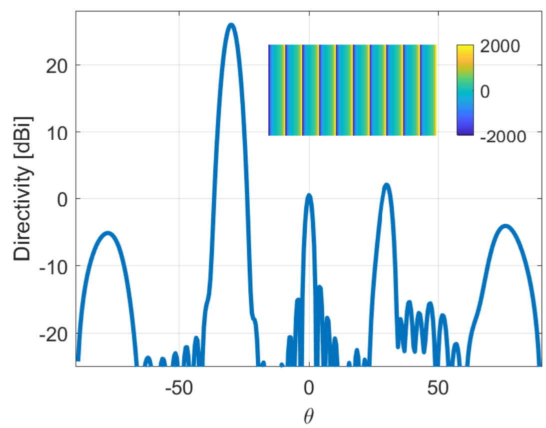

Fig. 9. Radiation pattern of a 10-period RIS generating anomalous reflection at 30°, considering a Gaussian field incident from broadside. The inset provides the imaginary part of the sheet impedance.

which can be expressed as $\mathcal{D}\{\mathbf{Z}_G - \mathbf{Z}_{IBC}\}^{-1}$, applied to the initial system of equations deteriorates the convergence.

The radiation pattern and the equivalent currents computed with the proposed algorithm are now compared with the ones obtained using an in-house MoM code (based on a direct solution of the system of equations) in Figs. 6 and 7, respectively. Besides, a good agreement is obtained between currents. It can be observed that the broadside specular reflection has been canceled, and a pencil beam has been formed at an elevation angle $\theta_r = 20°$ from broadside. The in-house MoM code has already been validated in [37] and [38], where good comparisons were obtained with commercial software.

However, the proposed preconditioned iterative algorithm is significantly faster and requires much less memory. Indeed, on our single conventional computer, the proposed iterative method can deal with MTSs of size $18\lambda_0$, meshed with more than 250 000 basis functions, in less than 45 min. The brute force code is limited to about 30 000 basis functions for memory reasons and even then already requires multiple hours of calculation. Next, a broadside impinging plane wave excitation is considered, and the system of equations is again solved. In this case, the specular reflection has been obtained with the PO approximation as explained in [39]. The resulting radiation pattern is shown in Fig. 8 along with an inset showing the convergence of the proposed system of equations. The required number of iterations is three times larger than the one associated with the Gaussian beam excitation, showing that a different excitation vector can impact the number of iterations. However, the system of equations still converges very well after preconditioning.

RISs implemented with the sheet impedance given by (31) usually produce undesired sidelobes which can be related to additional Floquet modes [40]. The RIS shown in the inset of Fig. 6 supports approximately two periods of the sheet impedance. Consequently, the sidelobes corresponding to the Floquet modes do not clearly appear due to the small size of the RIS. However, the modes start to appear when considering larger RISs. For example, the radiation pattern of Fig. 9 is obtained with an RIS supporting 10 periods. In this case, the sidelobes corresponding to Floquet modes clearly appear. This RIS is analyzed with 63 920 basis functions. Given the high number of unknowns, direct solution of the system of equations is impractical on a conventional computer. However, using the presented method, the iterative solver reaches a norm of residue of 10^{-6} in about 5 min.

The performance of the algorithm is now analyzed with respect to the size of the RIS. To do so, the sheet impedance of the previous example is selected, and the domain of the RIS is gradually increased while observing the simulation time and

TABLE II
EVALUATION TIME OF THE PROPOSED METHOD ON A SINGLE STANDARD COMPUTER

Size of the RIS	Number of unknowns	Green's function tabulation [min]	$\mathbf{Z}_G$ filling time [min]	$\mathbf{D}^{GG}$ filling time [min]	$\mathbf{Z}_{IBC}$ filling time [min]	$\mathbf{D}^{IBC}$ filling time [min]	Perform block inverse in (19) [min]	GMRES solving time [min]
$10\ \lambda_0 \times 10\ \lambda_0$	79600	0.938	0.33	0.044	0.015	0.03	0.022	3.58
$12\ \lambda_0 \times 12\ \lambda_0$	114720	1.12	0.48	0.094	0.021	0.06	0.04	5.58
$14\ \lambda_0 \times 14\ \lambda_0$	156240	1.4	0.7	0.16	0.033	0.1	0.053	12.8
$16\ \lambda_0 \times 16\ \lambda_0$	204160	1.45	0.9	0.25	0.038	0.15	0.078	24.9
$18\ \lambda_0 \times 18\ \lambda_0$	258480	1.76	1.075	0.284	0.045	0.2	0.1	42.6

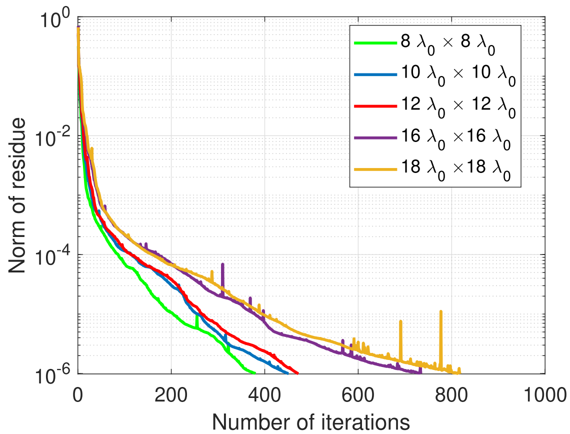

Fig. 10. Convergence of the method with respect to the structure size.

the convergence of the method. We consider a square-shaped RIS and we solve the system of equations (30). It is shown in Fig. 10 that the method still converges well when the size of the structure and hence the number of unknowns increases. The main steps and their respective computational times using a single standard computer (Intel Core i5-7500 3.4 GHz and 24 GB of RAM) are given in Table II.

B. Leaky Wave MTS Antenna Analysis

This section is devoted to the analysis of leaky wave MTS antennas [8]. This class of antenna usually implements a modulated capacitive sheet impedance. As shown in [16], a low reactance capacitive MTS exhibits a slow convergence due to the poor conditioning of the system of equations matrix. A low reactance capacitive sheet impedance may be required to increase the feed efficiency [19] or to facilitate the surface impedance implementation with an adopted set of patches. In this section, the convergence of the proposed method is analyzed considering squared-shape MTSs operating at 19 GHz with a low reactance capacitive sheet impedance lying on a substrate with relative permittivity $\epsilon_r = 6$ and thickness $d = 1.5$ mm. The antenna is excited with a vertical elementary dipole placed in the middle of the substrate and in the center of the aperture. An anisotropic sheet impedance profile is considered [8]

$$\begin{aligned} Z^{\rho\rho} &= jX_0\left[1 + M\cos\left(k_{sw}\rho - \phi\right)\right] \\ Z^{\rho\phi} &= Z^{\phi\rho} = jX_0 M\sin\left(k_{sw}\rho - \phi\right) \\ Z^{\phi\phi} &= jX_0\left[1 - M\cos\left(k_{sw}\rho - \phi\right)\right] \end{aligned} \tag{33}$$

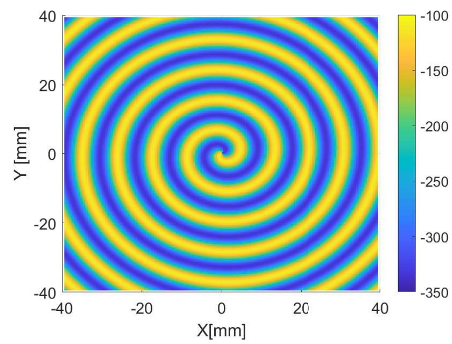

Fig. 11. Imaginary part of the $Z^{\rho\rho}$ component of the impedance profile given in (33).

with the following parameters: $X_0 = -222.42\ \Omega$, $M = 0.5$, and $k_{sw} = 1.8\ k_0$, where k_0 is the free-space wavenumber. (ρ, ϕ) corresponds to the polar system of coordinates centered on the MTS aperture. The $Z^{\rho\rho}$ component of this impedance profile is depicted in Fig. 11.

The GMRES solver is applied with two different sizes for the square-shaped MTS antenna: $5\lambda_0$ and $7\lambda_0$, meshed with 19 800 and 38 920 rooftop basis functions, respectively. The convergence of the preconditioned system of equations (30) is compared with the one of the initial system of equations (6) in Fig. 12, the latter with and without the diagonal preconditioner. As observed, a faster convergence is obtained using the proposed preconditioner. Again, the application of a simple diagonal preconditioner to the initial system of equations (6) significantly deteriorates the convergence.

The radiation pattern obtained after analyzing the MTS of size $5\lambda_0$ is now compared with that resulting from a direct inversion of the system of equations matrix (6) in Fig. 13. Indeed, this MTS is described with 19 800 basis functions; a system of equations of that size can still be directly solved on a standard computer. An excellent agreement between the patterns is observed, thus validating the proposed iterative solution.

C. Sparse Array MTS

In this section, we use the proposed preconditioner to analyze a $5\lambda \times 14\lambda$ MTS for which the initial MoM system of equations is ill-conditioned, and we validate the result at the printed patch level. Therefore, we consider the design proposed in [41] with the scalar surface impedance given by [41, Eq. (8)]. This impedance profile spans both capacitive and inductive ranges and leads to an ill-conditioned IBC-EFIE

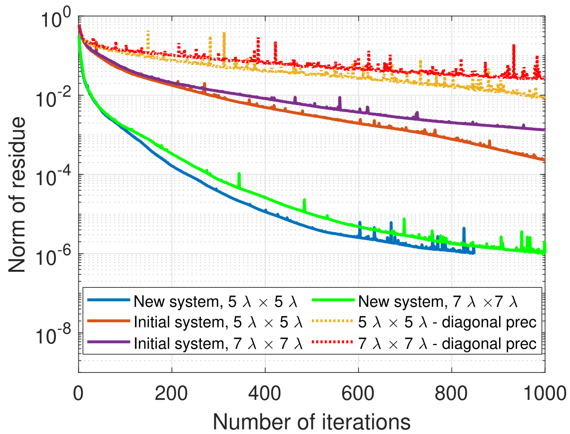

Fig. 12. Convergence of the proposed method compared to the convergence of the initial system of equations with and without the diagonal preconditioner for the low reactance capacitive square-shaped MTS antenna.

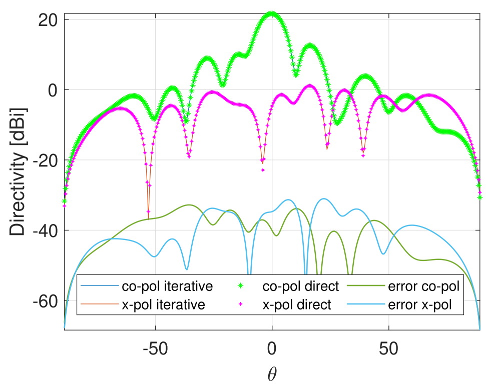

Fig. 13. Radiation pattern of the low reactance capacitive square-shaped MTS antenna of size $5\lambda_0 \times 5\lambda_0$, obtained with the iterative solver and with the direct method. The absolute error between patterns (in dB) is also provided.

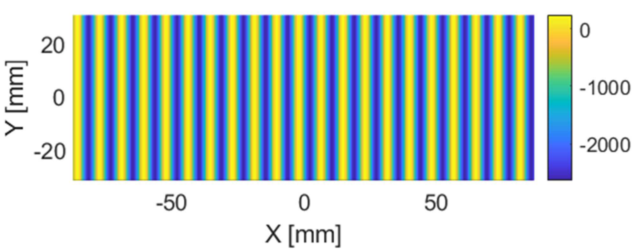

(a)

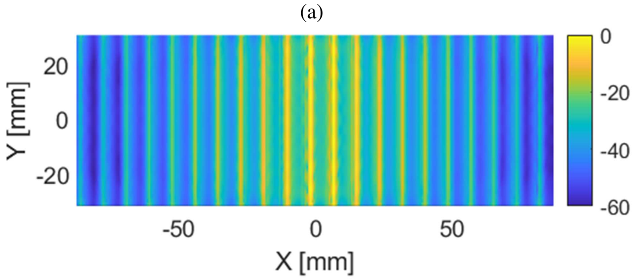

(b)

Fig. 14. Sparse array MTS proposed in [41]: (a) imaginary part of the impedance profile and (b) normalized equivalent currents.

system of equations. The proposed preconditioner is used to solve the latter. The impedance profile and the corresponding surface currents are shown in Fig. 14(a) and (b), respectively.

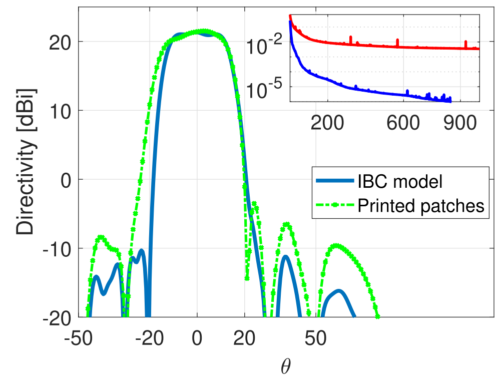

Fig. 15. Radiation pattern of the sparse array MTS proposed in [41] obtained with the proposed preconditioner at the IBC level and compared with the one obtained at the printed patch level in [41]. The inset shows the convergence (norm of residue versus number of iterations) of the present method (blue line) compared to the convergence of the initial system of equations (red line).

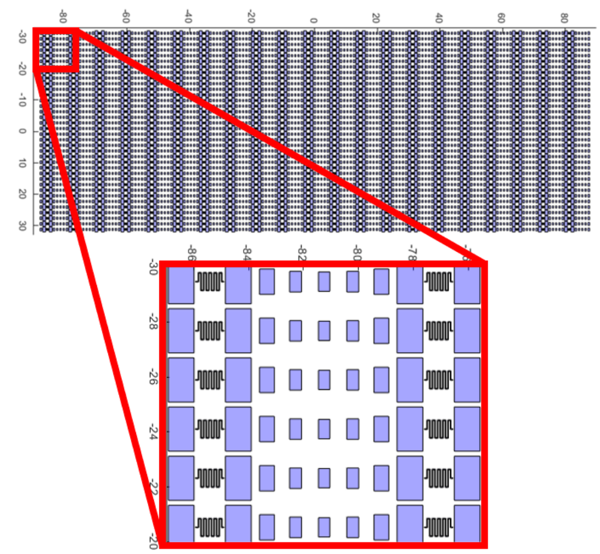

Fig. 16. Implementation of the sparse array MTS proposed in [41] at the patch level.

The resulting radiation pattern is shown in Fig. 15 where it is compared to the one obtained considering a full-wave analysis of the metasurface described at the patch level, which is shown in Fig. 16. More details regarding the patch implementation of the sparse array MTS can be found in [41]. In Fig. 15, an inset is provided with the convergence of the proposed method. This example shows that the method can be used to solve an ill-conditioned IBC-EFIE system of equations for which the solution agrees well with that of the EFIE when considering the printed patch implementation.

VI. Conclusion

Analyzing structures at the sheet impedance level has often led to ill-conditioning when the range of impedance spans both the capacitive and inductive domains. Therefore, a well-conditioned MoM technique is proposed for the fast analysis of MTS modeled as a modulated sheet impedance boundary condition. The solution of the system of equations matrix is obtained iteratively with the GMRES method. At each iteration, FFTs are used to accelerate the matrix–vector multiplication with the EFIE-IBC matrix and with its conjugate ($O(N \log N$ complexity). An additional matrix–vector multiplication with a block diagonal matrix is performed ($O(N^{3/2})$ complexity, considering a square-shaped domain). This matrix is precalculated using FFTs. The proposed preconditioner ensures a rapid convergence of the algorithm, whatever the range of the sheet impedance profile. As shown in the article, this method can be used to analyze large MTSs or RISs described with more than 250 000 basis functions with a conventional computer.

Acknowledgment

Views and opinions expressed are, however, those of the author(s) only and do not necessarily reflect those of the European Union. Neither the European Union nor the granting authority can be held responsible for them.

References

[1] X. Cao, Q. Chen, T. Tanaka, M. Kozai, and H. Minami, "A 1-bit time-modulated reflectarray for reconfigurable-intelligent-surface applications," *IEEE Trans. Antennas Propag.*, vol. 71, no. 3, pp. 2396–2408, Mar. 2023.

[2] M. Faenzi et al., "Metasurface antennas: New models, applications and realizations," *Sci. Rep.*, vol. 9, no. 1, p. 10178, Jul. 2019.

[3] Q. Wu, S. Zhang, B. Zheng, C. You, and R. Zhang, "Intelligent reflecting surface-aided wireless communications: A tutorial," *IEEE Trans. Commun.*, vol. 69, no. 5, pp. 3313–3351, May 2021.

[4] M. Bodehou, K. A. Khalifeh, S. N. Jha, and C. Craeye, "Direct numerical inversion methods for the design of surface wave-based metasurface antennas: Fundamentals, realizations, and perspectives," *IEEE Antennas Propag. Mag.*, vol. 64, no. 4, pp. 24–36, Aug. 2022.

[5] Y. Xie et al., "Anomalous refraction and reflection characteristics of bend V-shaped antenna metasurfaces," *Sci. Rep.*, vol. 9, no. 1, p. 6700, Apr. 2019.

[6] H. F. Ma, Y. Q. Liu, K. Luan, and T. J. Cui, "Multi-beam reflections with flexible control of polarizations by using anisotropic metasurfaces," *Sci. Rep.*, vol. 6, no. 1, p. 39390, Dec. 2016.

[7] J. L. Keyrouz, V. G. Ataloglou, and G. V. Eleftheriades, "Experimental demonstration of a dual-input/dual-output reflective impedance metasurface," *Appl. Phys. Lett.*, vol. 123, no. 16, Oct. 2023, Art. no. 161701.

[8] G. Minatti et al., "Modulated metasurface antennas for space: Synthesis, analysis and realizations," *IEEE Trans. Antennas Propag.*, vol. 63, no. 4, pp. 1288–1300, Apr. 2015.

[9] D. González-Ovejero, G. Minatti, G. Chattopadhyay, and S. Maci, "Multibeam by metasurface antennas," *IEEE Trans. Antennas Propag.*, vol. 65, no. 6, pp. 2923–2930, Jun. 2017.

[10] M. Bodehou, E. Martini, S. Maci, I. Huynen, and C. Craeye, "Multibeam and beam scanning with modulated metasurfaces," *IEEE Trans. Antennas Propag.*, vol. 68, no. 3, pp. 1273–1281, Mar. 2020.

[11] C. Yepes, S. Maci, S. A. Tretyakov, and E. Martini, "On the role of spatial dispersion in boundary conditions for perfect non-specular reflection," *EPJ Appl. Metamater.*, vol. 9, p. 17, Jul. 2022.

[12] M. A. Francavilla, E. Martini, S. Maci, and G. Vecchi, "On the numerical simulation of metasurfaces with impedance boundary condition integral equations," *IEEE Trans. Antennas Propag.*, vol. 63, no. 5, pp. 2153–2161, May 2015.

[13] F. Verni, M. Righero, and G. Vecchi, "On the use of entire-domain basis functions and fast factorizations for the design of modulated metasurface," *IEEE Trans. Antennas Propag.*, vol. 68, no. 5, pp. 3824–3833, May 2020.

[14] D. González-Ovejero and S. Maci, "Gaussian ring basis functions for the analysis of modulated metasurface antennas," *IEEE Trans. Antennas Propag.*, vol. 63, no. 9, pp. 3982–3993, Sep. 2015.

[15] M. Bodehou, D. González-Ovejero, C. Craeye, and I. Huynen, "Method of moments simulation of modulated metasurface antennas with a set of orthogonal entire-domain basis functions," *IEEE Trans. Antennas Propag.*, vol. 67, no. 2, pp. 1119–1130, Feb. 2019.

[16] J. Cavillot, M. Bodehou, S. Hubert, and C. Craeye, "Efficient analysis of planar, arbitrarily shaped, and (Bi)-anisotropic metasurface antennas," *IEEE Trans. Antennas Propag.*, vol. 70, no. 1, pp. 536–546, Jan. 2022.

[17] R. F. Harrington, *Field Computation by Moment Methods*. Piscataway, NJ, USA: IEEE Press, 1993.

[18] C. Yepes, M. Faenzi, S. Maci, and E. Martini, "Perfect non-specular reflection with polarization control by using a locally passive metasurface sheet on a grounded dielectric slab," *Appl. Phys. Lett.*, vol. 118, no. 23, Jun. 2021, Art. no. 231601.

[19] G. Minatti, E. Martini, and S. Maci, "Efficiency of metasurface antennas," *IEEE Trans. Antennas Propag.*, vol. 65, no. 4, pp. 1532–1541, Apr. 2017.

[20] S. B. Adrian, A. Dély, D. Consoli, A. Merlini, and F. P. Andriulli, "Electromagnetic integral equations: Insights in conditioning and preconditioning," *IEEE Open J. Antennas Propag.*, vol. 2, pp. 1143–1174, 2021.

[21] R. W. Kindt, K. Sertel, E. Topsakal, and J. L. Volakis, "Array decomposition method for the accurate analysis of finite arrays," *IEEE Trans. Antennas Propag.*, vol. 51, no. 6, pp. 1364–1372, Jun. 2003.

[22] P. Janpugdee, P. H. Pathak, P. Mahachoklertwattana, and R. J. Burkholder, "An accelerated DFT-MoM for the analysis of large finite periodic antenna arrays," *IEEE Trans. Antennas Propag.*, vol. 54, no. 1, pp. 279–283, Jan. 2006.

[23] D. Pissoort, E. Michielssen, D. Vande Ginste, and F. Olyslager, "A rank-revealing preconditioner for the fast integral-equation-based characterization of electromagnetic crystal devices," *Microw. Opt. Technol. Lett.*, vol. 48, no. 4, pp. 783–789, Apr. 2006.

[24] D. Tihon, S. Hubert, C. Craeye, and N. A. Ozdemir, "SVD post-compression combined with shielded-block preconditioner," in *Proc. Int. Conf. Electromagn. Adv. Appl. (ICEAA)*, Palm Beach, Aruba, Aug. 2014, pp. 503–506.

[25] S. Hubert, S. N. Jha, and C. Craeye, "Analysis of large nonregular printed scatterers using the contour-FFT," *IEEE Trans. Antennas Propag.*, vol. 66, no. 11, pp. 6115–6127, Nov. 2018.

[26] G. C. Hsiao and R. E. Kleinman, "Mathematical foundations for error estimation in numerical solutions of integral equations in electromagnetics," *IEEE Trans. Antennas Propag.*, vol. 45, no. 3, pp. 316–328, Mar. 1997.

[27] F. P. Andriulli et al., "A multiplicative Calderon preconditioner for the electric field integral equation," *IEEE Trans. Antennas Propag.*, vol. 56, no. 8, pp. 2398–2412, Aug. 2008.

[28] A. Dély, F. P. Andriulli, and K. Cools, "An impedance boundary condition EFIE that is low-frequency and refinement stable," *IEEE Trans. Antennas Propag.*, vol. 65, no. 3, pp. 1259–1266, Mar. 2017.

[29] M. Bruliard, M. Zucchi, and G. Vecchi, "Stability analysis of the EFIE-IBC formulation and regularization via spatial filtering," *IEEE Open J. Antennas Propag.*, vol. 6, pp. 578–593, 2025.

[30] X. Antoine and M. Darbas, "An introduction to operator preconditioning for the fast iterative integral equation solution of time-harmonic scattering problems," *Multiscale Sci. Eng.*, vol. 3, no. 1, pp. 1–35, Feb. 2021.

[31] J. Cavillot and C. Craeye, "A preconditioner for the fast analysis of arbitrarily-shaped reflective intelligent surfaces," in *Proc. 19th Eur. Conf. Antennas Propag. (EuCAP)*, Stockholm, Sweden, Mar. 2025, pp. 1–4.

[32] A. Glisson and D. Wilton, "Simple and efficient numerical methods for problems of electromagnetic radiation and scattering from surfaces," *IEEE Trans. Antennas Propag.*, vol. AP-28, no. 5, pp. 593–603, Sep. 1980.

[33] V. Y. Pan, *Structured Matrices Polynomials: Unified Superfast Algorithms*. New York, NY, USA: Springer, 2001.

[34] Y. Saad and M. H. Schultz, "GMRES: A generalized minimal residual algorithm for solving nonsymmetric linear systems," *SIAM J. Sci. Stat. Comput.*, vol. 7, no. 3, pp. 856–869, Jul. 1986.

[35] M. Bruliard, M. Righero, and G. Vecchi, "Stabilization of the integral equation for modelling metasurfaces via impedance boundary conditions," in *Proc. IEEE Int. Symp. Antennas Propag. USNC-URSI Radio Sci. Meeting (USNC-URSI)*, Portland, OR, USA, Jul. 2023, pp. 597–598.

[36] V. S. Asadchy, M. Albooyeh, S. N. Tcvetkova, A. Díaz-Rubio, Y. Ra'di, and S. A. Tretyakov, "Perfect control of reflection and refraction using spatially dispersive metasurfaces," *Phys. Rev. B, Condens. Matter*, vol. 94, no. 7, Aug. 2016, Art. no. 075142.

[37] H. V. Bui, S. N. Jha, and C. Craeye, "Fast full-wave synthesis of printed antenna arrays including mutual coupling," *IEEE Trans. Antennas Propag.*, vol. 64, no. 12, pp. 5163–5171, Dec. 2016.

[38] J. Cavillot, M. Bodehou, and C. Craeye, "Metasurface antennas design: Full-wave feeder modeling and far-field optimization," *IEEE Trans. Antennas Propag.*, vol. 71, no. 1, pp. 39–49, Jan. 2023.

[39] A. Abazi, J. Cavillot, and C. Craeye, "A method of moments approach for the simulation of truncated RIS," in *Proc. 19th Eur. Conf. Antennas Propag. (EuCAP)*, Stockholm, Sweden, Mar. 2025, pp. 1–4.
[40] A. Díaz-Rubio and S. A. Tretyakov, "Macroscopic modeling of anomalously reflecting metasurfaces: Angular response and far-field scattering," *IEEE Trans. Antennas Propag.*, vol. 69, no. 10, pp. 6560–6571, Oct. 2021.
[41] J. Dessy, M. Bodehou, J. Cavillot, and C. Craeye, "Sparse-array metasurface for beam scanning," *IEEE Trans. Antennas Propag.*, vol. 72, no. 10, pp. 8088–8093, Oct. 2024.

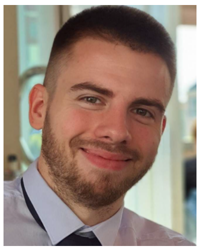

Jean Cavillot (Member, IEEE) was born in Arlon, Belgium, in 1994. He received the Ph.D. degree from the Université catholique de Leuven (UCLouvain), Ottignies-Louvain-la-Neuve, Belgium, in 2021.

Since 2021, he has occupied a Post-Doctoral Researcher position in UCLouvain, where he has been working on multiple projects involving the design and analysis of metasurface antennas and reflective surfaces. His thesis was focused on the fast numerical analysis of large structures involving planar media and was conducted under the FRIA grant from FNRS. His current research interests also include the fast analysis of large finite arrays.

Modeste Bodehou (Member, IEEE) was born in Cotonou, Benin, in 1992. He received the B.Sc. degree in engineering and the M.Sc. degree in electrical engineering (telecommunications) from the Royal Military Academy, Brussels, Belgium, in 2013 and 2015, respectively, the Ph.D. degree in engineering and technology, and the master's degree in management from the Université catholique de Leuven, Leuven-la-Neuve, Belgium, in 2020 and 2022, respectively.

In 2015, he was with the Quartier Major Housiau (Belgium Defense), Vilvoorde, Belgium, where he was involved in the framework of his application school on military communication systems. From 2020 to 2023, he was an FNRS Post-Doctoral Researcher in Belgium. He is currently an Assistant Professor with the Université d'Abomey-Calavi, Abomey-Calavi, Bénin. His current research interests include computational electromagnetics, antenna arrays, and metasurfaces.

Dr. Bodehou was a recipient of the 2024 IEEE AP-S Piergiorgio L.E. Uslenghi Letters Prize Paper Award, the 2023 Georges Vanderlinden Prize from the Belgian Royal Academy of Sciences, the 2021 EurAAP Per-Simon Kildal Award for Best Ph.D. in Antennas and Propagation, the Best Student Paper Award at the 13th European Conference on Antennas and Propagation, Krakow, Poland, 2019, the First Prize Student Paper Competition Award at the IEEE-MTTs International Conference on Numerical Electromagnetic and Multiphysics Modeling and Optimization for RF, Microwave, and Terahertz Applications, Seville, Spain, 2017, and the AIA Price for the Best Engineering Master Thesis Award from the Royal Military Academy, Brussels, 2015.

Adam Abazi (Graduate Student Member, IEEE) was born in Jette, Belgium, in 1999. He received the B.Sc. degree in engineering and the M.Sc. degree in electrical engineering from the Université catholique de Louvain (UCLouvain), Louvain-la-Neuve, Belgium, in 2020 and 2022, respectively, where he is currently pursuing the Ph.D. degree with the Antenna Group of ICTEAM.

His current research interests include the method of moments and the reconfigurable intelligent surfaces.

Christophe Craeye (Senior Member, IEEE) was born in Belgium, in 1971. He received the master's degree in electrical engineering and the B.Phil. degree from the Université Catholique de Louvain (UCLouvain), Ottignies-Louvain-la-Neuve, Belgium, in 1994, and the Ph.D. degree in applied sciences from UCLouvain, in 1998.

His Ph.D. was carried out in collaboration with the National Aeronautics and Space Administration (NASA) and the European Space Agency (ESA). From 1999 to 2001, he was a Post-Doctoral Researcher with the Eindhoven University of Technology, Eindhoven, The Netherlands. He was with the University of Massachusetts, Amherst, MA, USA, in 1999. He was with the Netherlands Institute for Research in Astronomy, Dwingeloo, The Netherlands, in 2001. In 2002, he started an antenna research activity with UCLouvain, where he is currently a Professor. He was with the Astrophysics and Detectors Group, University of Cambridge, Cambridge, U.K., in 2011. His research is funded by the Region Wallonne, the European Commission, ESA, the Fonds National de la Recherche Scientifique (FNRS), and UCLouvain. His current research interests include mutual coupling, finite antenna arrays, wideband antennas, small antennas, metasurfaces, and numerical methods for fields in periodic media, with applications to communication and sensing systems.

Dr. Craeye received the 2005–2008 Georges Vanderlinden Prize from the Belgian Royal Academy of Sciences in 2009. He was an Associate Editor of IEEE TRANSACTIONS ON ANTENNAS AND PROPAGATION, from 2004 to 2010, and IEEE ANTENNAS AND WIRELESS PROPAGATION LETTERS, from 2011 to 2017.